Reconciling spectroscopy with dynamics in global potential energy surfaces: the case of the astrophysically relevant SiC2

Monteiro Rocha, W.R.; Linnartz, H.V.J.; Varandas, A.J.C.

Note: To cite this publication please use the final published version (if applicable).

Reconciling spectroscopy with dynamics in global potential energy surfaces: The case of the astrophysically relevant SiC$_2$

C. M. R. Rocha, H. Linnartz and A. J. C. Varandas

View Online   Export Citation   CrossMark

ARTICLES YOU MAY BE INTERESTED IN

Reconciling spectroscopy with dynamics in global potential energy surfaces: The case of the astrophysically relevant SiC₂

View Online   Export Citation   CrossMark

C. M. R. Rocha,[1,a] H. Linnartz,[1] and A. J. C. Varandas[2,3,4]

AFFILIATIONS

[1] Laboratory for Astrophysics, Leiden Observatory, Leiden University, P.O. Box 9513, NL-2300 RA Leiden, The Netherlands
[2] School of Physics and Physical Engineering, Qufu Normal University, 273165 Qufu, China
[3] Department of Physics, Universidade Federal do Espírito Santo, 29075-910 Vitória, Brazil
[4] Department of Chemistry, and Chemistry Centre, University of Coimbra, 3004-535 Coimbra, Portugal

[a] Author to whom correspondence should be addressed: romerorocha@strw.leidenuniv.nl

ABSTRACT

SiC₂ is a fascinating molecule due to its unusual bonding and astrophysical importance. In this work, we report the first global potential energy surface (PES) for ground-state SiC₂ using the combined-hyperbolic-inverse-power-representation method and accurate *ab initio* energies. The calibration grid data are obtained via a general dual-level protocol developed afresh herein that entails both coupled-cluster and multi-reference configuration interaction energies jointly extrapolated to the complete basis set limit. Such an approach is specially devised to recover much of the spectroscopy from the PES, while still permitting a proper fragmentation of the system to allow for reaction dynamics studies. Besides describing accurately the valence strongly bound region that includes both the cyclic global minimum and isomerization barriers, the final analytic PES form is shown to properly reproduce dissociation energies, diatomic potentials, and long-range interactions at all asymptotic channels, in addition to naturally reflect the correct permutational symmetry of the potential. Bound vibrational state calculations have been carried out, unveiling an excellent match of the available experimental data on c-SiC₂($^1A_1$). To further exploit the global nature of the PES, exploratory quasi-classical trajectory calculations for the endothermic C₂ + Si → SiC + C reaction are also performed, yielding thermalized rate coefficients for temperatures up to 5000 K. The results hint for the prominence of this reaction in the innermost layers of the circumstellar envelopes around carbon-rich stars, hence conceivably playing therein a key contribution to the gas-phase formation of SiC, and eventually, solid SiC dust.

Published under an exclusive license by AIP Publishing. https://doi.org/10.1063/5.0096364

I. INTRODUCTION

Silicon dicarbide, SiC₂, has enjoyed a great deal of attention for its applications in astrochemistry:[1–14]

(i) Its most stable cyclic C_{2v} isomer, c-SiC₂($^1A_1$), was the first molecular ring identified in the interstellar medium.[1]

(ii) Its Merrill–Sanford band system ($\tilde{A}\,^1B_2$–$\tilde{X}\,^1A_1$ electronic transition) near 5000 Å was first observed in the optical absorption spectra of evolved stars and continues to be a particularly valuable astronomical probe of stellar atmospheres.[4,5]

(iii) Besides rovibronic transitions, the pure rotational signatures of both main (^{28}Si^{12}C₂) and singly substituted isotopologues (^{29}SiC₂, ^{30}SiC₂, and ^{28}Si^{13}CC) of c-SiC₂ have been identified in several astrophysical sources[1,2,6–8,10,11] and serve as sensitive molecular diagnostic tools for probing the chemical and physical conditions of the regions in which they reside.[1,6]

(iv) Together with SiC and Si₂C parent molecules, c-SiC₂ is ranked among the most likely gas-phase precursors leading to the formation of SiC dust grains in the inner envelopes of late-type carbon-rich stars.[9,10,12,13]

Apart from its intrinsic interest in an astronomical context, SiC₂ is also a fascinating molecule from a chemical viewpoint owing to its unique structure and dynamics.[15,16] Previous laboratory[15,17,18] and quantum mechanical studies[16,19–21] jointly provided ample evidence that its lowest energy C_{2v} minimum (as definitively assigned by Michalopoulos et al.[17]) has an exceedingly flat potential energy

surface (PES) along the internal rotation of the C_2 moiety within the molecule.[15–21] Such an untypical, nondirectional Si–C_2 bonding in c-SiC_2 (with reportedly high ionic character) has been classified[16,22] as polytopic[23] in nature and, hence, characterized by the nearly free circumnavigation of Si about C_2.[23] Indeed, the expectedly low energy difference between c-SiC_2 and the linear $C_{\infty v}$ (ℓ-SiCC) saddle-point structure was first confirmed experimentally by Ross et al.[15] as being only ∼ 1883 cm^{-1}. Clearly, like in C_3,[24,25] the expected high vibrational state populations and their delocalization over large regions of the PES make c-SiC_2's intramolecular motion lying at the borderlines of spectroscopy and chemical dynamics.

The conclusions drawn from these early experimental works by Michalopoulos et al.[17] and Ross et al.[15] motivated a plethora of detailed spectroscopic studies on c-SiC_2 aiming to further characterize its spectral signatures in both microwave,[7,8,11,12,26] infrared,[27–29] and optical[18,30] regions; for a comprehensive review, see Ref. 30 and references therein.

From the theoretical perspective, several concurring investigations were also ignited toward unraveling the SiC_2's unusual polytopic bonding nature and its large-amplitude dynamics;[16,19–22,31–33] for a complete account of the earlier theoretical literature, the reader is addressed to Refs. 16 and 21. In the most recent studies by Fortenberry et al.[20] and Koput,[21] special emphasis were put into the characterization of the c-SiC_2's local PES using state-of-the-art ab initio composite methods. By relying on the so-called CcCR protocol,[20] Fortenberry et al. reported a near-equilibrium quartic force field (QFF) for silicon dicarbide; the QFF was based on CCSD(T) energies extrapolated to the complete basis set (CBS) limit, augmented by additive corrections due to core-electron correlation and relativistic effects.[20] Using standard vibrational perturbational theory (VPT2), the CcCR QFF has shown to reproduce the c-SiC_2's stretching fundamentals (v_1 and v_2) to within 5 cm^{-1} of experiment,[18] whereas larger deviations of up to 21 cm^{-1} have been found for the v_3 (C_2 hindered rotation) mode.[20] As noted by Nielsen et al.[16] and Koput,[21] this is not surprising given the inherent deficiencies of VPT2 in properly describing such highly anharmonic, large-amplitude pinwheel dynamics of c-SiC_2. In the most sophisticated theoretical study to date by Koput,[21] a more extended PES [hereinafter referred to as Jacek Koput (JK) PES] was reported that describes locally not only c-SiC_2 but also the ℓ-SiCC saddle-point, in addition to the minimum energy path (MEP) connecting them; the calibration dataset included ab initio CCSD(T)-F12b/cc-pCVQZ-F12 energies additively corrected for higher-order valence–electron correlation beyond CCSD(T) and scalar relativistic effects.[21] Its barrier to linearity was predicted to be 1782 cm^{-1} which is lower than the previous high-level ab initio estimates by Nielsen et al.[16] (2030 cm^{-1}), and Kenny et al.[19] (2210 cm^{-1}), but closer to the experimental value[15] of 1883 cm^{-1}. Based on a variational approach, Koput[21] also performed bound-state calculations on his final potential; the results have shown that the JK PES is capable of reproducing the c-SiC_2's experimental vibrational term values reported by Ross et al.[15] with a root-mean-square deviation (rmsd) of ∼5 cm^{-1}.

Clearly, all the above distinctive features of SiC_2 make it a challenging testing ground for any theoretical methodological development. Moreover, the expected implications its unique spectroscopy and reaction dynamics might have in molecular astrophysics,

render this molecule a tempting target for further studies. As noted above, previous theoretical studies were mainly concerned with the determination of locally valid spectroscopic potentials for c-SiC_2[16,20,21] and there is not as yet a global PES for the title system that is capable of accurately describing both its valence and dissociation features at once. In this work, we delve deeper into the silicon dicarbide saga[16] and provide for the first time such a form for ground-state SiC_2. To allow for both bound-state and reaction dynamics calculations, the PES will be based on an accurate ab initio protocol that incorporates the best of two worlds: coupled-cluster [CCSD(T)] and multi-reference configuration interaction [MRCI(Q)] energies jointly extrapolated to the CBS limit. For the analytical modeling, we employ the Combined-Hyperbolic-Inverse-Power-Representation (CHIPR) method[34–37] as implemented in the CHIPR-4.0 program.[37] The quality of the final potential is further judged via both spectroscopic and exploratory reaction dynamics calculations.

II. METHODOLOGY

A. *Ab initio* calculations

All electronic structure calculations have been done with MOLPRO.[38] To ensure an accurate description of both valence and long-range features of the PES, the full set of ab initio grid points were herein generated using a combination[39] of CCSD(T)[40–42] (CC for brevity) and MRCI(Q)[43] (MR) levels of theory. The first is specially devised to improve the spectroscopy of the global minimum and is limited [due to the well-known[39,43] erratic behavior of such single-reference method for stretched bond distances (Fig. 1)] to a small region of the PES near the c-SiC_2/ℓ-SiCC stationary points. The MR set is in turn responsible to cover the bulk of the PES,[43] being restricted to sample the fragmentation region and geometries with high T_1 and D_1 diagnostics[44,45] [e.g., those characterized by larger C–C bond distances, away from the equilibrium region; see Fig. 3(a)]. Both datasets were subsequently extrapolated
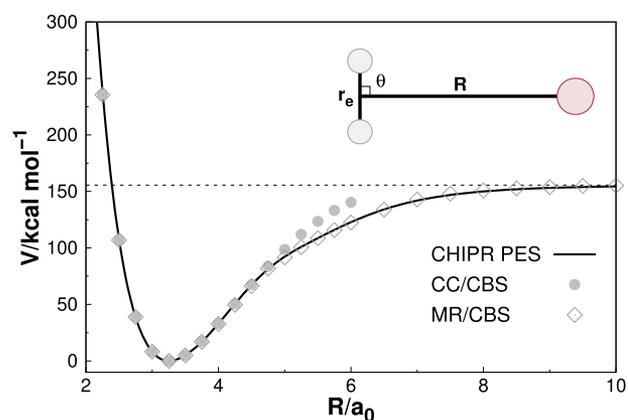
FIG. 1. Extrapolated CCSD(T) (CC/CBS) and MRCI(Q) (MR/CBS) energies for a cut along the perpendicular ($\theta = 90°$) approach of a Si atom into the C_2 diatomic with $r_e = 2.401\,33a_0$. The corresponding final CHIPR PES is also shown for comparison. The zero of energy corresponds to the T-shaped (C_{2v}) global minimum at $R = 3.253\,50a_0$.

to the CBS limit[46,47] (see below). The AVXZ ($X = T, Q, 5$) basis sets of Dunning and co-workers,[48,49] including additional tight-d functions ($+d$) for the Si atom,[38] were employed throughout.

At each selected geometry $\mathbf{R}$, the CC/CBS energy was defined as[50]

$$E_\infty^{CC}(\mathbf{R}) = E_\infty^{HF}(\mathbf{R}) + E_\infty^{cor}(\mathbf{R}), \quad (1)$$

where E_∞^{HF} and E_∞^{cor} are the extrapolated HF and CC correlation (cor) components. In Eq. (1), E_∞^{HF} is obtained via a two-point extrapolation protocol[51]

$$E_X^{HF}(\mathbf{R}) = E_\infty^{HF}(\mathbf{R}) + Ae^{-\beta x}, \quad (2)$$

where $x = q$ (3.87), p (5.07) are hierarchical numbers[52,53] that parallel the traditional $X = Q, 5$ cardinal ones, $\beta = 1.62$, and E_∞^{HF} and A are parameters to be calibrated from the raw RHF/AVXZ ($X = Q, 5$) energies.[51] In turn, E_∞^{cor} is obtained using the inverse-power formula[52]

$$E_X^{cor}(\mathbf{R}) = E_\infty^{cor}(\mathbf{R}) + \frac{A_3}{x^3}, \quad (3)$$

where q (3.68), p (4.71) are CC-type x numbers,[52] with E_∞^{cor} and A_3 calibrated from the raw CC/AVXZ ($X = Q, 5$) cor energies.

Similarly to Eq. (1), the CBS extrapolations of MR energies were performed individually for the non-dynamical (CAS) and dynamical (dc) correlations[54]

$$E_\infty^{MR}(\mathbf{R}) = E_\infty^{CAS}(\mathbf{R}) + E_\infty^{dc}(\mathbf{R}), \quad (4)$$

where E_∞^{CAS} is obtained using Eq. (2) but with CASSCF(12,12)/AVXZ ($X = T, Q$) raw energies[51] and E_∞^{dc} is given by the two-point law[55]

$$E_X^{dc}(\mathbf{R}) = E_\infty^{dc}(\mathbf{R}) + \frac{A_3}{(X-3/8)^3} + \frac{A_5^o + cA_3^{5/4}}{(X-3/8)^5}. \quad (5)$$

Here, A_5^o and c are universal type parameters,[55] and E_∞^{dc} and A_3 are obtained from the raw MRCI(Q)/AVXZ ($X = T, Q$) dc energies. The full-valence CASSCF active space includes the 3s- and 3p-like orbitals of Si and the 2s- and 2p-like orbitals of the C atoms. Note that, in the CC calculations, core correlation was not taken into account as this would imply, for reasons of consistency between both datasets, the consideration of such effects also at MR level, making the task of obtaining the global PES computationally unaffordable with current available resources. Thus, in all CC and MR calculations, only the valence electrons were correlated, with the 2s- and 2p-like orbitals of Si being included into the core.

Using the above dual-level CC/MR CBS protocol, a total of 3682 symmetry unique points (1144 and 2538 at CC/CBS and MR/CBS levels, respectively) have been selected to map all relevant regions of the ground-state PES of SiC$_2$ using atom–diatom Jacobi coordinates[56] (r, R, and θ in Fig. 1); the ranges are $2.0 \leq R/a_0 \leq 15.0$, $2.0 \leq r/a_0 \leq 3.5$, and $0.0 \leq \theta/\deg \leq 90.0$ for the Si–C$_2$ channel and $1.2 \leq R/a_0 \leq 15.0$, $2.8 \leq r/a_0 \leq 4.3$, and $0.0 \leq \theta/\deg \leq 180.0$ for C–SiC interactions. Recall that, in partitioning the nuclear configuration space, the CC/CBS dataset was chosen to cover only a limited region around the global minimum (including ℓ-SiCC), while the

MR/CC method was utilized elsewhere. Note that the corresponding C$_2$ and SiC curves were obtained solely at the MR/CBS level by making atom–diatom calculations with the Si and C atoms $50a_0$ far apart, varying the diatomic internuclear distance only; the total number of computed points for each curve amounts to ~ 63 and covers the coordinate range of $1.0 \leq r/a_0 \leq 50$. The reader is addressed to Figs. 3(a) and Figs. S1 and S2 of the supplementary material to assess the full set of *ab initio* grid points.

Finally, it should be noted that, while the use of larger basis sets would be desirable in estimating the CBS limits in Eqs. (1)–(5), preliminary test calculations have shown that the associated computational cost to obtain the full global PES would be nearly three times as high if the cardinal numbers in the above extrapolation formulas were increased by one unit. Because our proposed MR/CBS(T, Q) and CC/CBS($Q, 5$) protocols have already shown excellent performances when assessed against benchmark CBS energies,[46,47,51–53,55] we deeemed that there was no reason to extend the one-particle bases further.

B. Calibration of CHIPR PES

Within the CHIPR[34–37] formalism, the global adiabatic PES of ground-state SiC$_2$($^1A'$) assumes the following many-body expansion form:[56]

$$V(\mathbf{R}) = V_{C_2}^{(2)}(R_1) + V_{SiC}^{(2)}(R_2) + V_{SiC}^{(2)}(R_3) + V_{SiC_2}^{(3)}(\mathbf{R}), \quad (6)$$

where the $V^{(2)}$'s represent the diatomic (two-body) potentials of C$_2$($a^3\Pi_u$) and SiC($X^3\Pi$), and $V^{(3)}$ is the three-body term; $\mathbf{R} = \{R_1, R_2, R_3\}$ is the set of interatomic separations, with the energy zero set to the infinitely separated C(^3P)+C(^3P)+Si(^3P) atoms. As Eq. (6) indicates, our analytic CHIPR PES dissociates adiabatically into C$_2$($a^3\Pi_u$)+Si(^3P) and SiC($X^3\Pi$)+C(^3P), hence modeling only the lowest electronic singlet state of SiC$_2$ correlating to such open shell fragments; this is warranted by including in Eq. (6), the proper diatomic two-body terms and ensuring that $V^{(3)}$ naturally vanishes for large interatomic separations.[36,37] Note that, similarly to C$_3$,[24,25] the ground-state singlet PES of SiC$_2$ does not dissociate adiabatically into ground-state C$_2$($X^1\Sigma_g^+$)+Si(^3P) fragments which, according to spin-correlation rules,[57] correlate with the triplet manifold of SiC$_2$ states; see Fig. S3 for further details. Note further that the spin-allowed C$_2$($X^1\Sigma_g^+$)+Si(^1D) channel lies[58,59] ≈ 16 kcal mol^{-1} above the C$_2$($a^3\Pi_u$)+Si(^3P) asymptote and correlates with excited singlet PESs.[24,25]

In Eq. (6), the CHIPR diatomic curves are expressed by the general form[37]

$$V^{(2)}(R) = \frac{Z_A Z_B}{R} \sum_{k=1}^{L} C_k y^k, \quad (7)$$

where Z_A and Z_B denote the nuclear charges of atoms A and B, and the C_k's are expansion coefficients; the y coordinate is herein defined as a linear combination of R-dependent basis functions[37] [see Eq. (9)]. In turn, $V^{(3)}$ in Eq. (6) is represented via CHIPR's three-body model which for AB$_2$-type species assumes the simplified form[35,37,61]

$$V^{(3)}(\mathbf{R}) = \sum_{i,j,k=0}^{L} C_{i,j,k} \left[y_1^i (y_2^j y_3^k + y_2^k y_3^j) \right]. \quad (8)$$

In the above equation, $C_{i,j,k}$ are expansion coefficients of a Lth-degree polynomial, and the y_p's ($p = 1, 2, 3$) are (transformed) coordinates. These latter are expressed in terms of distributed-origin contracted basis sets[37]

$$y_p = \left(\sum_{\alpha=1}^{M-1} c_\alpha \phi_{p,\alpha}^{[1]} \right) + c_M \phi_{p,M}^{[2]}, \tag{9}$$

where

$$\phi_{p,\alpha}^{[1]} = \text{sech}\left[\xi_{p,\alpha} \left(R_p - R_{p,\alpha}^{\text{ref}} \right) \right] \tag{10}$$

and

$$\phi_{p,M}^{[2]} = \left[\frac{\tanh\left(\frac{1}{5} R_p \right)}{R_p} \right]^6 \text{sech}\left[\xi_{p,M} \left(R_p - R_{p,\alpha}^{\text{ref}} \right) \right] \tag{11}$$

are primitive bases with origin at R^{ref} and the ξ's are non-linear parameters. All steps involved in the calibration of Eqs. (7)–(11) using *ab initio* data points are fully described in Refs. 36 and 37, with the reader being addressed to them for further details. Note that, to obtain the global analytic form of the PES [Eq. (6)], we herein employ the newly developed CHIPR-4.0 program.[37] With this code, the final CHIPR diatomic potentials of C_2 and SiC [Eq. (7)] were calibrated using MR/CBS points with rmsd's of 1.1 and 0.3 cm^{-1}, respectively. For completeness, they are plotted in Fig. S1. As for the three-body term, all 3682 *ab initio* dual-level CC/MR CBS points could be least-squares fitted to Eq. (8) with chemical accuracy (rmsd = 0.9 kcal mol^{-1}). The weights (W) so employed were: $W = 1$ for calculated points with energies $E \leq 50$ kcal mol^{-1} above the global C_{2v} minimum, $W = 0.7$ for those within the interval $50 < E/\text{kcal mol}^{-1} \leq 135$, and $W = 0.2$ for geometries with $E > 135$ kcal mol^{-1} above c-SiC$_2$. Our fit involves a total of 180 linear coefficients in the polynomial expansion [$L = 11$ in Eq. (8)]; see Tables S1–S4 of the supplementary material to access the numerical coefficients of all parameters resulting from the fit. Figure S2 also portrays some representative cuts of the final analytic CHIPR potential [Eq. (6)] alongside the corresponding *ab initio* ones. Table I displays the stratified rmsd, while Fig. 2

TABLE I. Stratified root-mean-square deviations (in kcal mol^{-1}) of the final PES.

Energy[a]	N[b]	Max. dev.[c]	rmsd	$N_{>\text{rmsd}}$[d]
50	804	1.5	0.2	156
100	1102	3.0	0.3	179
150	2088	3.5	0.5	249
200	2723	5.0	0.8	453
250	3430	5.1	0.9	588
500	3578	5.1	0.9	658
1200	3682	5.1	0.9	680

[a]The units of energy are kcal mol^{-1}. Energy strata defined with respect to the C_{2v} absolute minimum of SiC$_2$: $-364.993\,433$ E$_h$ at CCSD(T)/CBS level. Its relative energy (as predicted from the PES with respect to the infinitely separated C + C + Si atoms) is $-0.474\,269$ E$_h$.
[b]Number of calculated points up to indicated energy range.
[c]Maximum deviation up to indicated energy range.
[d]Number of calculated points with an energy deviation larger than the rmsd.
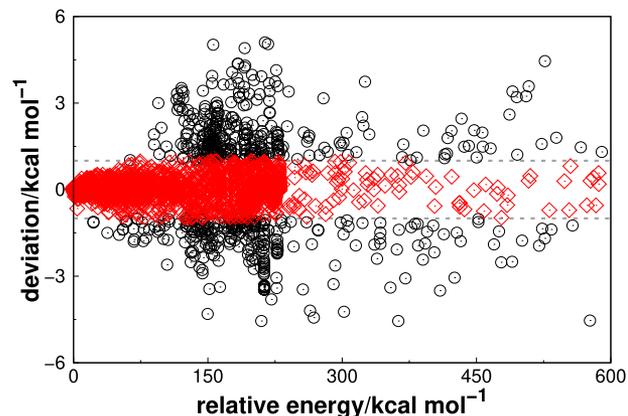
FIG. 2. Scatter plot of deviations between fitted [using the CHIPR model function of Eq. (6)] and calculated *ab initio* energies as a function of the total energy. In the x axis, the zero is set relative to the C_{2v} global minimum of SiC$_2$. Points fitted with chemical accuracy ($|\text{deviation}| \leq 1$ kcal mol^{-1}) are represented in red.

shows the distribution of errors of the fitted dataset. Accordingly, we note that ∼82% of the data are herein fitted with 0.9 kcal mol^{-1} accuracy. Moreover, Fig. 2 indicates that most of the calculated grid points (95% of the total population) are primarily distributed within the 300 kcal mol^{-1} range above c-SiC$_2$, hence approximately spanning the energy interval of up to its complete atomization[62,63] (if we consider the atom + diatom geometries utilized to calibrate the diatomic curves). The high-energy points, particularly those within $300 < E/\text{kcal mol}^{-1} \leq 1200$ (see Table I and Fig. 2), are characterized by short CC and/or SiC bond distances which, despite carrying lower weights in the least-squares fitting procedure (see above), are shown to be important to properly model the repulsive walls of the global potential, preventing the three-body term [$V^{(3)}$ in Eq. (6)] from attaining large negative values at these regions.

In relation to our combined CC/MR protocol, we should mention that, despite being extrapolated to the CBS limit, the two *ab initio* theories unavoidably diverge, especially at long distances; a prototypical case is illustrated in Fig. 1. This latter is clearly due to the single-reference CC which is not expected to properly describe dissociation.[43] These CC points, whenever present, were eliminated from the fit, warranting a smooth transition between the two datasets and the lowest rmsd; see Figs. 1 and S2. In the valence region, correlation energy differences between CC and MR also exist (even at CBS limit) but are less evident (Fig. 1), showing the smallest deviations near the global minimum; for example, at c-SiC$_2$, the CC/CBS and MR/CBS total energies differ by ∼71 μEh, a value that compares quite well with the corresponding estimate of ∼11 μEh calculated using CCSD(T)-F12b/VQZ-F12 and MRCI(Q)-F12/VQZ-F12 energies. These inherent discrepancies in CC and MR correlation energies are expected to increase when going up in energy, likely attaining larger values at long-range distances (Fig. 1). Note, however, that, because the low-energy part of our potential is primarily sampled by CC/CBS points [Fig. 3(a)], we expect that the existence of such a CC/MR seam (lying higher in energy) influences little the final spectroscopic properties of the PES to be discussed next.
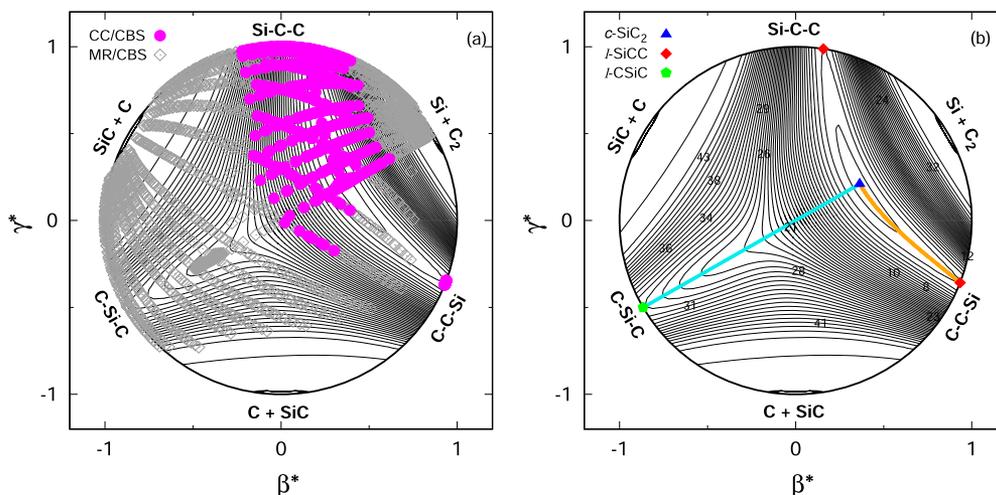
FIG. 3. Relaxed-triangular plot in scaled hyperspherical coordinates[60] [$\beta^\star$ and $\gamma^\star$; see Eq. (12)] of the ground-state CHIPR PES of SiC$_2$ showing (a) the distribution of *ab initio* CCSD(T)/CBS (magenta solid circles) and MRCI(Q)/CBS (gray open diamonds) calibration dataset; (b) its global topographical attributes, location of stationary points (indicated by symbols), and isomerization pathways shown later in 1D in Fig. 6. In both plots, linear geometries lie at the border of the physical circle, while the C_{2v} line connects Si + C$_2$ to *c*-SiC$_2$ to ℓ-CSiC. The origin ($\beta^\star$ = 0 and $\gamma^\star$ = 0) defines a D_{3h} configuration and C_s structures are elsewhere. The location of all atom + diatom dissociation channels is properly indicated. Contours are equally spaced by 0.007 E$_h$ starting at −0.5 E$_h$. The zero of energy is set relative to the infinitely separated C + C + Si atoms. The corresponding 3D version of plot (b) is shown later in Fig. 8.

III. FEATURES OF PES

All major features of the final CHIPR PES are depicted in Figs. 3–8. The properties of its stationary points are collected in Table II wherein the most accurate results from the literature[1,15,17,18,20,21] as well as our own *ab initio* CC and MR values are also included for comparison. Note that, to allow for a complete visualization of all topographical attributes of our global CHIPR analytic potential, Fig. 3 shows a relaxed-triangular contour plot in scaled hyperspherical coordinates,[60] $\beta^\star = \beta/Q$ and $\gamma^\star = \gamma/Q$, where

$$\begin{pmatrix} Q \\ \beta \\ \gamma \end{pmatrix} = \begin{pmatrix} 1 & 1 & 1 \\ 0 & \sqrt{3} & -\sqrt{3} \\ 2 & -1 & -1 \end{pmatrix} \begin{pmatrix} R_1^2 \\ R_2^2 \\ R_3^2 \end{pmatrix}, \qquad (12)$$

and R_1, R_2, and R_3 are interatomic distances. Thus, by relaxing the "size" Q of the molecule such as to give the lowest energy for a given "shape" (β and γ) of the triangle formed by the three atoms, the contour plot shown in Fig. 3 is then obtained; see legend therein and Refs. 39 and 24 for further details. The corresponding 3D version of this plot is shown later in Fig. 8. In turn, Figs. 4 and 5 illustrate the PES for the Si and C atoms moving around relaxed C$_2$ and SiC fragments, respectively. They also summarize in a comprehensive manner all predicted stationary structures from the analytic CHIPR PES to be discussed next.

A. Valence region and spectroscopic calculations

According to Figs. 3–8, the predicted global minimum on the ground-state singlet PES corresponds to a cyclic C_{2v} geometry, *c*-SiC$_2$($^1A_1$). As Table II shows, its characteristic bond lengths and angle are R_1(Si–C) = R_2(Si–C) = 3.468 a$_0$ and

$\alpha(\angle$ C–Si– C) = 40.5°. These values are in excellent agreement with the most reliable theoretical estimates due to Fortenberry *et al.*[20] and Koput,[21] differing by less than 0.008 a$_0$/0.1°. Recall that these authors include, in addition to CBS energies, contributions from core–core/core–valence electron correlation and scalar relativistic effects in their local PESs; Koput[21] further accounts for higher-order $\mathcal{N}$-particle electron correlation beyond CCSD(T). Close agreement is also found between the CHIPR's *c*-SiC$_2$ data and experimental attributes taken from the literature;[1,15,17,18] see Table II. Indeed, our predicted C–C (ν_1) and Si–C (ν_2) stretching fundamentals reproduce exceedingly well ($\lesssim$ 3.5 cm^{-1}) the corresponding experimental values[15] and are quite consistent with those calculated from the JK PES (Table II). Yet, larger discrepancies (of up to 16 cm^{-1}) are found for the large-amplitude ν_3 fundamental associated with the internal rotation of the C$_2$ moiety. As noted elsewhere,[16,21] the proper description of the expectedly highly anharmonic potential along this mode [Figs. 4 and 6(a)] requires an iterative treatment of the connected triples (T_3) and quadruples (T_4) correlation contributions in the coupled-cluster expansion; this, however, would make the task of calculating the global PES of SiC$_2$ computationally unfeasible, even if limited to a smaller section of PES near *c*-SiC$_2$ [Fig. 3(a)]. Indeed, the corresponding ν_3 value reported by Koput[21] differs by less than 3 cm^{-1} from its experimental estimate. Despite the expected lower performance of CHIPR relative to JK in predicting ν_3, we note that our variationally computed fundamentals for *c*-SiC$_2$ still appear to be slightly more accurate than those reported using the CcCR QFF/VPT2 protocol,[20] even without considering here relativistic and core-valence correlation effects; see Table II.

To further assess the accuracy of the final CHIPR PES, we have carried out anharmonic vibrational calculations for higher excited modes using the DVR3D software suite[65] and compared the results

TABLE II. Structural equilibrium parameters (in valence coordinates, R_i in a_0, α in degrees), harmonic (ω_i) and fundamental (v_i) frequencies (in cm^{-1}) of the stationary points on the ground-state singlet PES of SiC_2. Relative energies (ΔE) are in kcal mol^{-1} and given with respect to the C_{2v} global minimum.

Structure	Method[a]	R_1	R_2	α	ΔE[a]	ω_1 (v_1)	ω_2 (v_2)	ω_3 (v_3)
c-SiC_2	CC/AVQZ	3.478	3.478	40.5	0.0	1763.9	807.9	180.5
	MR/AVQZ	3.488	3.488	40.6	0.0	1743.9	793.2	223.2
	CC/CBS[b]				0.0			
	MR/CBS[b]				0.0			
	CcCR QFF[c]	3.460	3.460	40.5		1781.9 (1750.5)	815.1 (844.7)	201.4 (175.4)
	JK PES[d]	3.460	3.460	40.6	0.0	1776.1 (1745.6)	812.7 (837.9)	214.6 (194.1)
	CHIPR PES	3.468	3.468	40.5	0.0	1804.4 (1749.4)	823.2 (840.1)	201.6 (180.4)
	Expt.	3.459[e]	3.459[e]	40.6[e]	0.0	1756.8[f] (1746.0)[g]	844.0[f] (840.6)[g]	(196.4)[g]
ℓ-SiCC	CC/AVQZ	2.434	3.206	180.0	4.8	1887.9	787.4	81.9i
	MR/AVQZ	2.456	3.231	180.0	4.2	1846.3	765.7	55.7i
	CC/CBS[b]				5.4			
	MR/CBS[b]				4.5			
	JK PES[d]	2.425	3.192	180.0	5.1	1901.4	790.5	82.6i
	CHIPR PES	2.430	3.202	180.0	5.4	1893.6	783.5	102.1i
	Expt.				5.4 ± 0.6[h]			
ℓ-CSiC	CC/AVQZ	3.401	3.401	180.0	131.6	947.6	707.5	177.8i
	MR/AVQZ	3.431	3.431	180.0	128.1	912.3	690.5	162.6i
	CC/CBS[b]				132.8			
	MR/CBS[b]				129.2			
	CHIPR PES	3.409	3.409	180.0	129.2	902.8	729.2	112.9i

[a]This work, unless stated otherwise.
[b]CC/CBS and MR/CBS single-point energies calculated at CHIPR PES stationary points.
[c]Quartic force field of Ref. 20.
[d]Jacek Koput (JK) local PES of Ref. 21.
[e]Experimental equilibrium parameters reported in Ref. 20. The corresponding zero-point values are[64] $R_{1,0} = R_{2,0} = 3.463 a_0$ and $\alpha_0 = 40.505°$.
[f]Experimental harmonic frequencies taken from Ref. 18.
[g]Experimental fundamental frequencies taken from Ref. 15.
[h]Potential energy barrier determined by Ross et al.[15] from experimental data.

with the experimental term energies reported by Ross et al.[15] All calculated data are gathered in Table III. Also shown for comparison are the corresponding values reported from the JK local PES.[21] Note that the vibrational band origins cover energies up to about 5200 cm^{-1} (6600 cm^{-1}) above the ground-state zero-point level (bottom of the well) of c-SiC_2 and excitations of up to as high as 16 quanta in v_3; the approximate quantum numbers v_1 and v_2 refer to the C–C and Si–C stretching vibrations, while v_3 corresponds to the antisymmetric stretching of the triangular geometry. The results presented in Table III show that our CHIPR PES reproduces remarkably well the vibrational spectrum of c-SiC_2 with a rmsd of 16 cm^{-1} (as expected, the largest deviations are ascribed to overtones and combination bands involving v_3). This is quite astounding given the global, purely *ab initio* nature of the PES and is clearly an asset of the present dual-level CC/MR protocol.[39] It should be stressed that such a mixed protocol is herein devised to improve the spectroscopy of global potentials relative to global PESs calibrated solely using MR grid energies. Indeed, our experience shows (see, e.g., Refs. 66 and 25) that purely MR global forms, despite accurately describing the bulk of the PESs, do in general a relatively poor job at reproducing experimental vibrational band origins of triatomics, showing rmsd's of

~50 cm^{-1} or even greater. We reiterate that the lower performance of CHIPR when compared to the accurate JK local PES (see Table III) is not surprising given the absence of higher-order effects in our CC calibration data, in addition to the fact that global analytic forms unavoidably entail larger fitting errors, even near the global minimum. In turn and differently from CHIPR, the JK potential cannot physically describe all dissociation channels and may show spurious features at regions of the PES characterized by large C–C bond distances. Additionally, CHIPR describes by built-in the complete atomization of the system. Considering the c-SiC_2's anharmonic zero-point energy (1400.1 cm^{-1}) and its stabilization energy relative to the C + C + Si atoms ($-0.474 269 E_h$), a total atomization energy of 293.6 kcal mol^{-1} is predicted from our PES. This value is in excellent agreement with the best theoretical estimate of 293.1 kcal mol^{-1} reported by Oyedepo et al.[63] using the MR-ccCA protocol[63] and the early G2 result by Deutsch and Curtiss[62] (294.7 kcal mol^{-1}); the last known experimental value is[62] 301.0 ± 7 kcal mol^{-1}.

As Figs. 3(b) and 4 portray, c-SiC_2 is connected by two-symmetry equivalent linear ($C_{\infty v}$) transition states, ℓ-SiCC($^1\Sigma^+$), located at R_1(C–C) = 2.430 a_0, R_2(Si–C) = 3.202 a_0, and $\alpha(\angle Si$–C– C) = 180.0° with an imaginary frequency of 102.1 cm^{-1}.
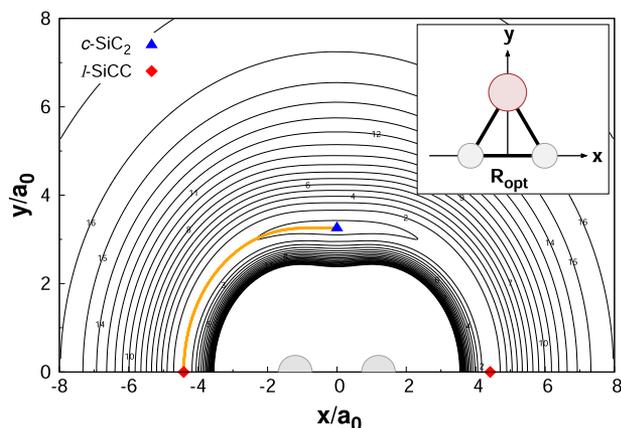
FIG. 4. CHIPR contour plot for a Si atom moving around a partially relaxed C_2 diatom ($2.2 \leqslant r/a_0 \leqslant 2.6$), which lies along the x axis with the center of the bond fixed at the origin. X and y coordinates give the position of Si with respect to the origin. Linear geometries are defined by $x \neq 0$ and $y = 0$, while the $x = 0$ and $y \neq 0$ line describes C_{2v} configurations; C_s structures are elsewhere. Contours are equally spaced by 0.015 E_h starting at -0.5 E_h. The zero of energy is set relative to the infinitely separated C + C + Si atoms. Solid color line represents the minimum energy path shown in 1D in Fig. 6(a).

The corresponding minimum energy path (MEP) calculated[67] from the PES is plotted in Fig. 6(a) and clearly represents the large-amplitude nearly free pinwheel motion of C_2 around Si. Indeed, a close look at Fig. 6(a) shows that the CHIPR form accurately reproduces the MEP at the CC/CBS level, with the corresponding MR/CBS path being actually lower in energy. Suffice it to say that such MR/CBS points are only shown therein for comparison – they were not included in the fit as this region is only sampled by CC/CBS points (Sec. II A). Our best theoretical estimate (taken from
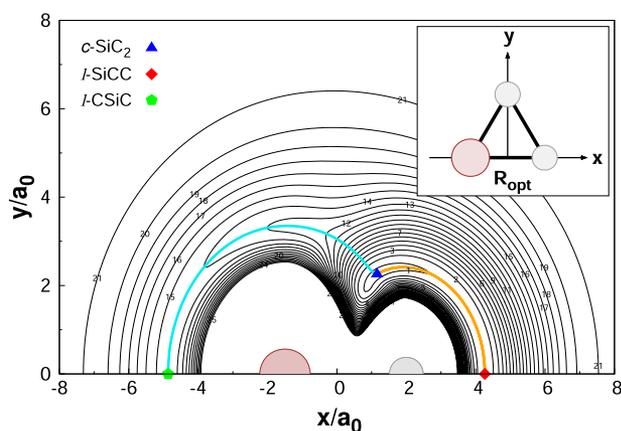
FIG. 5. CHIPR contour plot for a C atom moving around a partially relaxed SiC diatom ($3.0 \leqslant r/a_0 \leqslant 4.0$), which lies along the x axis with origin at its center of mass. x and y coordinates define the position of C with respect to the origin. Contours are equally spaced by 0.015 E_h starting at -0.5 E_h. The zero of energy is set relative to the infinitely separated C + C + Si atoms. Solid color lines represent the minimum energy paths shown in 1D in Figs. 6(a) and 6(b).
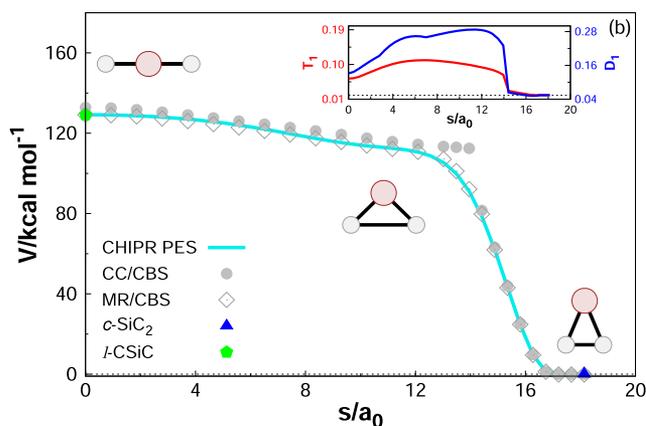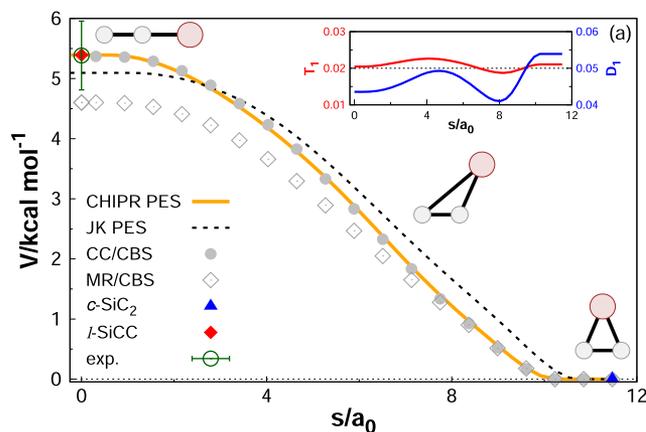
FIG. 6. CHIPR minimum energy paths (s are reaction coordinates in mass-scaled a.u.) and potential energy barriers for the conversion of c-SiC$_2$ to (a). ℓ-SiCC and (b). ℓ-CSiC configurations. Solid circles and open diamonds indicate *ab initio* CCSD(T)/CBS and MRCI(Q)/CBS single-point energies calculated at the predicted CHIPR geometries. In panel (a)., the corresponding path obtained using the Jacek Koput (JK) local PES[21] and the experimentally derived c-SiC$_2$ → ℓ-SiCC barrier reported by Ross *et al.*[15] are also shown for comparison. In panels (a) and (b), MRCI(Q)/CBS and CCSD(T)/CBS points, respectively, were not included in the fit and are only plotted for comparison. The insets display the evolution of the coupled-cluster T_1 and D_1 diagnostics along the underlying paths as obtained from CCSD(T)/AV5Z calculations.

the analytic PES) places ℓ-SiC$_2$ at 5.4 kcal mol^{-1} (1886.1 cm^{-1}) above c-SiC$_2$, in excellent agreement with the reported value of 5.1 kcal mol^{-1} (1781.9 cm^{-1}) by Koput.[21] Most notably, our predicted barrier to linearity is shown to match nearly perfectly the corresponding experimental estimate of[15] 5.4 ± 0.6 kcal mol^{-1} (1883 ± 200 cm^{-1}). These results provide compelling evidence that, at this level, CC appears to be more reliable in describing the c-SiC$_2$/ℓ-SiCC region, despite lying at the threshold of single-reference description with[44,45] $T_1 \sim 0.02$ and $D_1 \sim 0.05$; see the inset of Fig. 6(a). The corresponding barrier predicted at MR/CC level is ≈ 0.9 kcal mol^{-1} lower than the CC/CBS estimate (Table II), being nearly coincident with the value of 4.5 kcal mol^{-1} reported by Koput at MR-ACPF/cc-pV6Z level.[21]

TABLE III. Calculated and observed vibrational term values (in cm^{-1}) for c-SiC$_2$($^1A_1$).

					Calc	
v_1	v_2	v_3	Γ_{vib}	Obs[a]	CHIPR[b]	JK[c]
0	0	0	A_1	0.0	0.0	0.0
0	0	2	A_1	352.85	326.1	349.6
0	0	4	A_1	605.33	573.5	600.3
0	0	6	A_1	814.87	793.4	809.2
0	1	0	A_1	840.6	840.1	837.9
0	0	8	A_1	1013.5	997.6	1005.1
0	0	10	A_1	1185.0	1179.7	1179.2
0	1	2	A_1	1264.6	1239.0	1261.6
0	0	12	A_1	1350.48	1347.4	1342.6
0	0	14	A_1	1492.16	1490.4	1482.8
0	1	4	A_1	1556.7	1521.9	1549.0
0	0	16	A_1	1614.0	1625.5	1609.3
0	2	0	A_1	1667.8	1667.7	1665.2
1	0	0	A_1	1746.0	1749.4	1745.6
1	0	2	A_1	2078.0	2054.9	2075.1
1	0	4	A_1	2322.1	2297.4	2318.8
0	3	0	A_1	2465.7	2450.3	2460.4
1	0	6	A_1	2539.0	2521.6	2530.7
1	1	0	A_1	2579.2	2588.8	2580.0
1	0	8	A_1	2735.0	2733.6	2732.6
1	0	10	A_1	2918.0	2924.9	2916.1
0	4	0	A_1	3303.0	3292.4	3303.8
1	2	0	A_1	3406.6	3414.9	3405.6
2	0	0	A_1	3465.8	3464.2	3467.1
2	1	0	A_1	4299.0	4304.2	4299.7
2	2	0	A_1	5122.0	5125.0	5120.6
3	0	0	A_1	5164.0	5155.5	5163.4
0	0	1	B_1	196.37	180.4	194.1
0	0	3	B_1	487.2	454.9	482.6
0	0	5	B_1	717.6	686.7	709.7
0	1	1	B_1	917.7	898.0	910.4
0	0	7	B_1	1072.2	1060.7	1070.1
0	0	9	B_1	1107.3	1094.8	1100.1
0	1	3	B_1	1271.0	1266.1	1262.8
0	0	11	B_1	1412.0	1385.5	1404.8
0	0	13	B_1	1436.5	1425.7	1429.7
0	1	5	B_1	1558.0	1561.0	1550.2
0	0	15	B_1	1689.6	1686.1	1677.6
0	1	7	B_1	1883.0	1879.9	1877.6
1	0	1	B_1	1925.0	1917.5	1928.3
0	2	1	B_1	1955.0	1941.3	1955.6
1	0	3	B_1	2201.0	2179.3	2202.7
1	0	5	B_1	2430.0	2421.7	2428.8
1	0	7	B_1	2627.0	2628.8	2634.2
			rmsd[d]		16.0	5.3

[a] Experimental data from Ref. 15.
[b] Calculated using CHIPR PES and DVR3D.[65] The zero-point energy is 1400.1 cm^{-1}.
[c] Jacek Koput (JK) local PES. Data from Ref. 21.
[d] Root-mean-square deviations with respect to experimental data.

A notable aspect of the CHIPR PES, discussed previously in early studies,[31–33] is the existence of an auxiliary $D_{\infty h}$ transition state, ℓ-CSiC($^1_g\Sigma^+$). As Table II shows, this linear form has characteristic bond lengths of R_1(Si–C) = R_2(Si–C) = 3.409 a$_0$ and an imaginary frequency of 112.9 cm^{-1} along the bending coordinate. Its connection to c-SiC$_2$ is perhaps best seen from the contour plots in Figs. 3(b) and 5; see the cyan solid lines represented therein. The associated isomerization pathway[67] in $1D$ is presented in Fig. 6(b), wherein the major topographical valence attributes of the CHIPR PES across C_{2v} geometries can be assessed. Accordingly, ℓ-CSiC is predicted from our final CHIPR form to lie 129.2 kcal mol^{-1} above c-SiC$_2$. Differently from ℓ-SiCC that spans a low energy region of the PES primarily sampled by CC/CBS points [Fig. 3(a)], the description of ℓ-CSiC and vicinities can only be accurately done at MR/CBS level. In fact, as the inset of Fig. 6(b) shows, at this region of the nuclear configuration space the predicted CC diagnostics (e.g., $T_1 \approx 0.11$ and $D_1 \approx 0.27$ halfway through the MEP) far exceed the accepted limiting values: $T_1 \lesssim 0.02$,[44] $D_1 \lesssim 0.05$,[45] thus clearly entailing a multi-reference approach. This is explained by the presence of several low-lying excited electronic states in this region, as Fig. S3(a) illustrates. Indeed, Fig. 6(b) evinces that the CHIPR form mimics excellently well the *ab initio* MR/CBS data, with the predicted barrier to linearity matching exactly the one calculated at this level (Table II). We further note that, in Fig. 6(b), the CC/CBS data shown are only plotted for comparison; they were not included in the calibration dataset as this high-energy valence region of the PES (with $s \lesssim 15$ a$_0$) is sampled solely by MR/CBS calculations.

B. Proof of concept: Long-range region and reaction dynamics calculations

Apart from accurately modeling the valence (strongly bound) chemical space, the contour plots shown in Figs. 3–5 evidently pinpoint the reliability of the CHIPR form to describe long-range and dissociation features of the SiC$_2$ PES, in addition to naturally reflect its correct permutational symmetry. This is clearly an
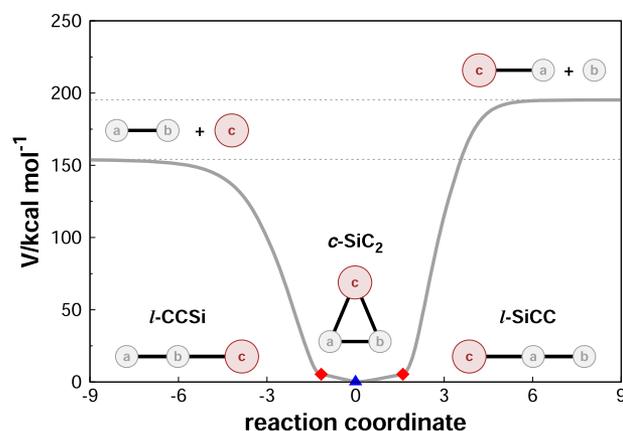
FIG. 7. $1D$ cut of the CHIPR PES along the minimum energy path connecting C$_2$ + Si and SiC + C via SiC$_2$ intermediates. Black dashed lines mark the associated energies of the infinitely separated atom + diatom fragments. The a, b, and c labels are introduced to distinguish between the symmetry-equivalent structures.

asset of the CHIPR[34–37] formalism [namely, Eq. (8)] and is the major deliverable of the present work. Figure 7 shows the calculated MEP for the chemical conversion of C_2 + Si to SiC + C that proceeds via SiC_2 intermediates. Accordingly, both forward and reverse collision processes evolve without activation barriers for collinear atom–diatom approaches, leading directly to the formation of ℓ-SiCC. This structure is subsequently converted to c-SiC_2 by way of low-energy (nearly free) C_2 internal rotations [Fig. 6(a)]; the stabilization energy of the c-SiC_2 complex is predicted to be ~−154.1 and −195.4 kcal mol^{-1} relative to the infinitely separated C_2 + Si and SiC + C fragments, respectively, this former being quite close to the value of −152.9 kcal mol^{-1} reported by Nielsen et al.[16] based on high-level focal point thermochemical analyses. Indeed, as Fig. 7 shows, the

C_2 + Si → SiC + C reaction is highly endothermic (40.4 kcal mol^{-1}, including the zero-point energies of the reactants and products) which makes this process feasible only in high-temperature environments, e.g., in the inner envelopes surrounding (late-type) carbon-rich stars,[10,12] hence conceivably playing therein a key role in the formation of gas-phase SiC, and consequently solid SiC dust. Initial assessments indicate that, in order to effectively initiate such a reaction, C_2 must be initially pumped[69] to higher vibrational states (up to at least v = 10–11) or collide with a high-energy Si atom, with relative translational energies of the order of ~ 41 kcal mol^{-1} or higher; see, e.g., Fig. 8. These conditions can be fulfilled within the inner layers of the circumstellar shells of evolved C-stars (e.g., IRC + 10 216) characterized by temperatures of ~1000 to 3000 K or higher and where $C_2(X^1\Sigma_g^+, a^3\Pi_u)$ and other silicon–carbon species are known to be particularly conspicuous.[12] To further assess the reliability of such a reaction, we have run preliminary quasi-classical trajectory (QCT) calculations[68,70] on the CHIPR PES using a locally modified version of the VENUS96C code;[68] for a thorough description of the methodology here utilized, see Ref. 71 and Table S5. At the high-temperature regime considered ($2000 \le T/K \le 5000$), the calculated thermal rate coefficients for C_2 + Si → SiC + C can be accurately represented by the Arrhenius–Kooij formula[72]

$$k(T) = A\left(\frac{T}{300}\right)^B \exp\left(\frac{-C}{T}\right),$$ (13)

where A = 1.225 82 × 10^{-10} cm^3 molecule^{-1} s^{-1}, B = −0.161 897, and C = 20 305.15 K. This is plotted in Fig. 9, together with the calculated QCT data which are numerically defined in Table S5. Accordingly, the theoretically predicted rate constants for C_2 + Si → SiC + C show a positive temperature dependence, increasing steeply from T = 3000 K. This provides compelling evidence for its relevance in the gas-phase synthesis of SiC and related solid SiC dust formation in the innermost envelopes of C-stars.[73] Further investigations
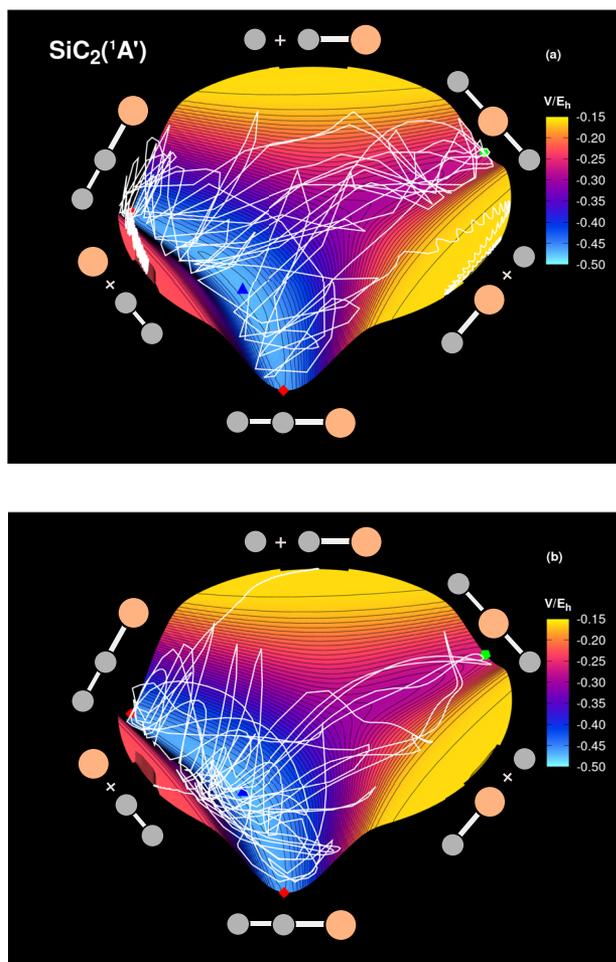
FIG. 8. Relaxed 3D hyperspherical plots [see also Fig. 3(b)] of the CHIPR PES of $SiC_2(^1A')$ showing the time evolution (in coordinate space) of sample reactive quasi-classical trajectories (solid white lines) calculated using the VENUS96C code[68] for $Si(^3P)+C_2(a^3\Pi_u)\rightarrow SiC(X^3\Pi)+C(^3P)$ with distinct initial conditions: (a) vibrationally excited $C_2(v = 11)$ and collision energy of 1.0 kcal mol^{-1} and (b) ground-state C_2 and collision energy of 42.0 kcal mol^{-1}. Stationary points and coordinates as in Fig. 3(b). The zero of energy is set relative to the infinitely separated C + C + Si atoms.
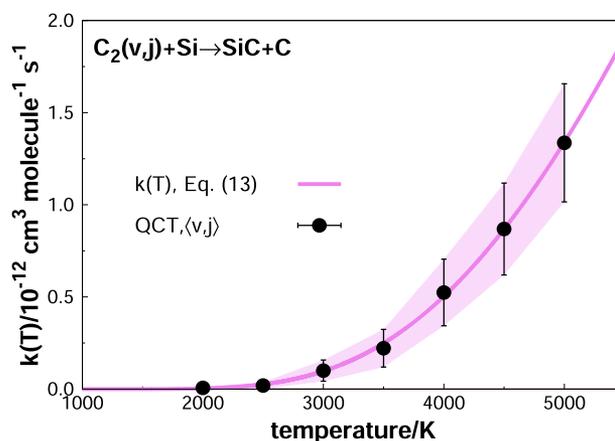
FIG. 9. Calculated rate constants and associated error bars for the $Si(^3P)$ +$C_2(a^3\Pi_u)\rightarrow SiC(X^3\Pi)+C(^3P)$ reaction within the temperature range of $2000 \le T/K \le 5000$. The lines show the predicted QCT thermally averaged results from Eq. (13). For clarity, the QCT results are shown with 99.6% (3σ) error bars.

in this direction are in order and a detailed account of the overall $C_2 + Si \rightarrow SiC + C$ dynamics and kinetics undoubtedly requires a careful assessment of the possible contributions of other excited-states PESs correlating to the same reactant/product channels; this is clearly beyond the scope of our present preliminary analysis and will be the focus of future studies. Also of relevance is the reverse (barrierless and exothermic) $SiC + C \rightarrow C_2 + Si$ reaction (Fig. 7) which, differently from $C_2 + Si \rightarrow SiC + C$, surely occurs at cold and ultra-cold temperatures, hence dominated by long-range forces; indeed, the expected high reactivity of SiC with[74] atomic C and O at low Ts may help explain the lack of SiC detections in cold interstellar environments.[75–77]

IV. CONCLUSIONS

We report the first global PES for ground-state $SiC_2(^1A')$ based on CBS extrapolated *ab initio* energies and the CHIPR method for the analytical modeling. By relying on a mixed CCSD(T) and MRCI(Q) protocol, we ensure that the final potential recovers much of the spectroscopy of its cyclic global minimum, while still permitting an accurate description of isomerization and fragmentation processes, all with the correct permutational symmetry as naturally warranted by CHIPR. Bound-state calculations performed anew have shown that the present purely *ab initio* CHIPR PES is capable of reproducing the experimental vibrational spectrum of cyclic SiC_2 with a rmsd of 16 cm^{-1}. Despite not outperforming the spectroscopic quality of the most accurate local PES to date,[21] our proposed dual-level CCSD(T)/MRCI(Q) CBS protocol is expected to improve the spectroscopy of global ground-state PESs when compared with purely MRCI(Q)-based global forms. Further improvements can be so envisaged by either fine-tuning the theoretically predicted potential parameters with input experimental information[66,78] or morphing the original global form with a spectroscopically accurate local potential.[25] Aside from anharmonic vibrational calculations, the global nature of our CHIPR PES is further exploited by performing preliminary quasi-classical trajectory calculations for the $C_2 + Si \rightarrow SiC + C$ endothermic reaction. The calculated thermal rate coefficients within the temperature range of $2000 \leq T/K \leq 5000$ hint for its prominence in the gas-phase synthesis of SiC and, presumably, SiC dust formation in the inner envelopes surrounding carbon-rich stars.[10,12]

SUPPLEMENTARY MATERIAL

See the supplementary material to assess the performance of the PES alongside *ab initio* grid data, the numerical coefficients of the final CHIPR analytic form, as well as the calculated QCT reaction rate coefficients.

AUTHOR DECLARATIONS

Conflict of Interest

The authors have no conflicts to disclose.

Author Contributions

C. M. R. Rocha: Conceptualization (equal); Data curation (equal); Formal analysis (equal); Funding acquisition (equal); Investigation (equal); Visualization (equal); Writing – original draft (equal); Writing – review & editing (equal). **H. Linnartz**: Conceptualization (equal); Funding acquisition (equal); Resources (equal); Supervision (equal); Writing – original draft (equal); Writing – review & editing (equal). **A. J. C. Varandas**: Conceptualization (equal); Methodology (equal); Software (equal); Validation (equal); Writing – review & editing (equal).

DATA AVAILABILITY

The full set of *ab initio* grid points support the findings of this study are available from the corresponding author upon reasonable request. A Fortran subroutine of the final CHIPR PES that readily evaluates the potential and gradient at any arbitrary geometry is made available as supplementary material.

REFERENCES

[1] P. Thaddeus, S. E. Cummins, and R. A. Linke, "Identification of the SiCC radical toward IRC+10216: The first molecular ring in an astronomical source," Astrophys. J. **283**, L45–L48 (1984).

[2] L. A. Nyman, H. Olofsson, L. E. B. Johansson, R. S. Booth, U. Carlstrom, and R. Wolstencroft, "A molecular radio line survey of the carbon star IRAS 15194-5115," Astron. Astrophys. **269**, 377–389 (1993).

[3] P. D. Gensheimer and L. E. Snyder, "A search for vibrationally excited SiC_2 $v_3 = 1$ toward IRC + 10216," Astrophys. J. **490**, 819–822 (1997).

[4] P. J. Sarre, M. E. Hurst, and T. Lloyd Evans, "SiC_2 in carbon stars: Merrill-Sanford absorption bands between 4100 and 5500 Å," Mon. Not. R. Astron. Soc. **319**, 103–110 (2000).

[5] D. H. Morgan, D. Hatzidimitriou, and R. D. Cannon, "Merrill-sanford bands in large magellanic cloud carbon stars," Mon. Not. R. Astron. Soc. **355**, 1196–1206 (2004).

[6] J. Cernicharo, L. B. F. M. Waters, L. Decin, P. Encrenaz, A. G. G. M. Tielens, M. Agúndez, E. De Beck, H. S. P. Müller, J. R. Goicoechea, M. J. Barlow, A. Benz, N. Crimier, F. Daniel, A. M. Di Giorgio, M. Fich, T. Gaier, P. García-Lario, A. de Koter, T. Khouri, R. Liseau, R. Lombaert, N. Erickson, J. R. Pardo, J. C. Pearson, R. Shipman, C. Sánchez Contreras, and D. Teyssier, "A high-resolution line survey of IRC + 10216 with Herschel/HIFI- first results: Detection of warm silicon dicarbide (SiC_2)," Astron. Astrophys. **521**, L8 (2010).

[7] D. L. Kokkin, S. Brünken, K. H. Young, N. A. Patel, C. A. Gottlieb, P. Thaddeus, and M. C. McCarthy, "The rotational spectra of $^{29}SiC_2$ and $^{30}SiC_2$," Astrophys. J., Suppl. Ser. **196**, 17 (2011).

[8] H. S. P. Müller, J. Cernicharo, M. Agúndez, L. Decin, P. Encrenaz, J. C. Pearson, D. Teyssier, and L. B. F. M. Waters, "Spectroscopic parameters for silacyclopropynylidene, SiC₂, from extensive astronomical observations toward CW Leo (IRC + 10216) with the Herschel satellite," J. Mol. Spectrosc. **271**, 50–55 (2012).

[9] D. Gobrecht, S. Cristallo, L. Piersanti, and S. T. Bromley, "Nucleation of small silicon carbide dust clusters in AGB stars," Astrophys. J. **840**, 117 (2017).

[10] S. Massalkhi, M. Agúndez, J. Cernicharo, L. Velilla Prieto, J. R. Goicoechea, G. Quintana-Lacaci, J. P. Fonfría, J. Alcolea, and V. Bujarrabal, "Abundance of SiC₂ in carbon star envelopes—Evidence that SiC₂ is a gas-phase precursor of SiC dust," Astron. Astrophys. **611**, A29 (2018).

[11] J. Cernicharo, M. Guélin, M. Agúndez, J. R. Pardo, S. Massalkhi, J. P. Fonfría, L. Velilla Prieto, G. Quintana-Lacaci, N. Marcelino, C. Marka, S. Navarro, and C. Kramer, "IRC + 10216 as a spectroscopic laboratory: Improved rotational constants for SiC₂, its isotopologues, and Si₂C," Astron. Astrophys. **618**, A4 (2018).

[12] M. C. McCarthy, C. A. Gottlieb, and J. Cernicharo, "Building blocks of dust: A coordinated laboratory and astronomical study of the archtype AGB carbon star IRC + 10216," J. Mol. Spectrosc. **356**, 7–20 (2019).

[13] M. Agúndez, J. I. Martínez, P. L. de Andres, J. Cernicharo, and J. A. Martín-Gago, "Chemical equilibrium in AGB atmospheres: Successes, failures, and prospects for small molecules, clusters, and condensates," Astron. Astrophys. **637**, A59 (2020).

[14] M. K. Sharma and A. K. Sharma, "Investigation of silicon dicarbide (SiC₂) in circumstellar envelopes around carbon-rich AGB stars," Indian J. Phys. **94**, 1869–1874 (2020).

[15] S. C. Ross, T. J. Butenhoff, E. A. Rohlfing, and C. M. Rohlfing, "SiC₂: A molecular pinwheel," J. Chem. Phys. **100**, 4110–4126 (1994).

[16] I. M. B. Nielsen, W. D. Allen, A. G. Császár, and H. F. Schaefer, "Toward resolution of the silicon dicarbide (SiC₂) saga: Ab initio excursions in the web of polytopism," J. Chem. Phys. **107**, 1195–1211 (1997).

[17] D. L. Michalopoulos, M. E. Geusic, P. R. R. Langridge-Smith, and R. E. Smalley, "Visible spectroscopy of jet-cooled SiC₂: Geometry and electronic structure," J. Chem. Phys. **80**, 3556–3560 (1984).

[18] T. J. Butenhoff and E. A. Rohlfing, "Laser-induced fluorescence spectroscopy of jet-cooled SiC₂," J. Chem. Phys. **95**, 1–8 (1991).

[19] J. P. Kenny, W. D. Allen, and H. F. Schaefer, "Complete basis set limit studies of conventional and R12 correlation methods: The silicon dicarbide (SiC₂) barrier to linearity," J. Chem. Phys. **118**, 7353–7365 (2003).

[20] R. C. Fortenberry, T. J. Lee, and H. S. P. Müller, "Excited vibrational level rotational constants for SiC₂: A sensitive molecular diagnostic for astrophysical conditions," Mol. Astrophys. **1**, 13–19 (2015).

[21] J. Koput, "Ab initio potential energy surface and vibration-rotation energy levels of silicon dicarbide, SiC₂," J. Comput. Chem. **37**, 2395–2402 (2016).

[22] J. Oddershede, J. R. Sabin, G. H. F. Diercksen, and N. E. Grüner, "The structure and spectrum of SiC₂," J. Chem. Phys. **83**, 1702–1708 (1985).

[23] E. Clementi, H. Kistenmacher, and H. Popkie, "Study of the electronic structure of molecules. XVIII. Interaction between a lithium atom and a cyano group as an example of a polytopic bond," J. Chem. Phys. **58**, 2460–2466 (1973).

[24] C. M. R. Rocha and A. J. C. Varandas, "Accurate ab initio-based double many-dody expansion potential energy surface for the adiabatic ground-state of the C₃ radical including combined Jahn-Teller plus pseudo-Jahn-Teller interactions," J. Chem. Phys. **143**, 074302–074318 (2015).

[25] C. M. R. Rocha and A. J. C. Varandas, "Energy-switching potential energy surface for ground-state C₃," Chem. Phys. Lett. **700**, 36–43 (2018).

[26] C. A. Gottlieb, J. M. Vrtilek, and P. Thaddeus, "Laboratory measurement of the rotational spectrum of SiCC," Astrophys. J., Lett. **343**, L29 (1989).

[27] R. A. Shepherd and W. R. M. Graham, "FTIR matrix isolation study of carbon-13 substituted SiC₂," J. Chem. Phys. **82**, 4788–4790 (1985).

[28] J. D. Presilla-Márquez, W. R. M. Graham, and R. A. Shepherd, "Fourier transform far infrared spectroscopy of the ν'₃ vibration of SiC₂ in Ar at 10 K," J. Chem. Phys. **93**, 5424–5428 (1990).

[29] M. Izuha, S. Yamamoto, and S. Saito, "Rotational spectrum of SiC₂ in the ν₃ excited state," Spectrochim. Acta, Part A **50**, 1371–1378 (1994).

[30] Q. Zhang, D.-P. Zhang, B.-X. Zhu, J.-W. Gu, C.-T. Yu, Z.-J. Xiao, Y. Chen, and D.-F. Zhao, "High-resolution spectroscopy of the 0_0^0, 2_0^1, 3_0^1 and 3_1^1 bands in the $\tilde{A}\,^1B_2$–$\tilde{X}\,^1A_1$ transition of SiC₂," J. Mol. Spectrosc. **372**, 111306 (2020).

[31] S. Green, "Theoretical study of silicon dicarbide," Astrophys. J. **266**, 895–901 (1983).

[32] S. Arulmozhiraja and P. Kolandaivel, "Four energetically low lying states of SiC₂," J. Mol. Struct.: THEOCHEM **334**, 71–79 (1995).

[33] Y. Zhang, C.-Y. Zhao, W.-H. Fang, and Z.-H. Lu, "High accuracy studies on the ground state and transition state of SiC₂," J. Mol. Struct.: THEOCHEM **454**, 31–40 (1998).

[34] A. J. C. Varandas, "Combined-hyperbolic-inverse-power-representation of potential energy surfaces: A preliminary assessment for H₃ and HO₂," J. Chem. Phys. **138**, 054120 (2013).

[35] A. J. C. Varandas, "Putting together the pieces: A global description of valence and long-range forces via combined hyperbolic inverse power representation of the potential energy surface," in Reaction Rate Constant Computations: Theories and Applications, edited by K. Han and T. Chu (The Royal Society of Chemistry, 2013), Chap. 17, pp. 408–445.

[36] C. M. R. Rocha and A. J. C. Varandas, "A general code for fitting global potential energy surfaces via CHIPR method: Triatomic molecules," Comput. Phys. Commun. **247**, 106913 (2020).

[37] C. M. R. Rocha and A. J. C. Varandas, "A general code for fitting global potential energy surfaces via CHIPR method: Direct-fit diatomic and tetratomic molecules," Comput. Phys. Commun. **258**, 107556 (2021).

[38] H. J. Werner, P. J. Knowles, G. Knizia, F. R. Manby, M. Schütz et al., "MOLPRO, a package of ab initio programs, version 2010.1," 2010, http://www.molpro.net, Cardiff.

[39] B. R. L. Galvão and A. J. C. Varandas, "Accurate double many-body expansion potential energy surface for N₃($^4A''$) from correlation scaled ab initio energies with extrapolation to the complete basis set limit," J. Phys. Chem. A **113**, 14424–14430 (2009).

[40] P. J. Knowles, C. Hampel, and H. J. Werner, "Coupled cluster theory for high spin, open shell reference wave functions," J. Chem. Phys. **99**, 5219–5227 (1993).

[41] P. Piecuch, M. Wloch, and A. J. C. Varandas, "Renormalized coupled-cluster methods: Theoretical foundations and application to the potential function of water," in Topics in the Theory of Chemical and Physical Systems, edited by S. Lahmar, J. Maruani, S. Wilson, and G. Delgado-Barrio (Springer Netherlands, Dordrecht, 2007), pp. 63–121.

[42] R. J. Bartlett and M. Musiał, "Coupled-cluster theory in quantum chemistry," Rev. Mod. Phys. **79**, 291–352 (2007).

[43] P. G. Szalay, T. Müller, G. Gidofalvi, H. Lischka, and R. Shepard, "Multiconfiguration self-consistent field and multireference configuration interaction methods and applications," Chem. Rev. **112**, 108–181 (2012).

[44] T. J. Lee and P. R. Taylor, "A diagnostic for determining the quality of single-reference electron correlation methods," Int. J. Quantum Chem. **36**, 199–207 (1989).

[45] C. L. Janssen and I. M. B. Nielsen, "New diagnostics for coupled-cluster and Møller-Plesset perturbation theory," Chem. Phys. Lett. **290**, 423–430 (1998).

[46] A. J. C. Varandas, "Straightening the hierarchical staircase for basis set extrapolations: A low-cost approach to high-accuracy computational chemistry," Annu. Rev. Chem. **69**, 177–203 (2018).

[47] A. J. C. Varandas, "Extrapolation in quantum chemistry: Insights on energetics and reaction dynamics," J. Theory Comput. Chem. **19**, 2030001 (2020).

[48] T. H. Dunning, "Gaussian basis sets for use in correlated molecular calculations. I. The atoms boron through neon and hydrogen," J. Chem. Phys. **90**, 1007–1023 (1989).

[49] R. A. Kendall, T. H. Dunning, and R. J. Harrison, "Electron affinities of the first-row atoms revisited. Systematic basis sets and wave functions," J. Chem. Phys. **96**, 6796–6806 (1992).

[50] C. M. R. Rocha and A. J. C. Varandas, "A global CHIPR potential energy surface for ground-state C₃H and exploratory dynamics studies of reaction C₂ + CH → C₃ + H," Phys. Chem. Chem. Phys. **21**, 24406–24418 (2019).

[51] F. N. N. Pansini, A. C. Neto, and A. J. C. Varandas, "Extrapolation of Hartree-Fock and multiconfiguration self-consistent-field energies to the complete basis set limit," Theor. Chem. Acc. **135**, 261–267 (2016).

[52] A. J. C. Varandas and F. N. N. Pansini, "Narrowing the error in electron correlation calculations by basis set re-hierarchization and use of the unified singlet and triplet electron-pair extrapolation scheme: Application to a test set of 106 systems," J. Chem. Phys. **141**, 224113 (2014).

[53] F. N. N. Pansini, A. C. Neto, and A. J. C. Varandas, "On the performance of various hierarchized bases in extrapolating the correlation energy to the complete basis set limit," Chem. Phys. Lett. **641**, 90–96 (2015).

[54] C. M. R. Rocha and A. J. C. Varandas, "Accurate CHIPR potential energy surface for the lowest triplet state of C_3," J. Phys. Chem. A **123**, 8154–8169 (2019).

[55] A. J. C. Varandas, "Extrapolating to the one-electron basis-set limit in electronic structure calculations," J. Chem. Phys. **126**, 244105 (2007).

[56] J. N. Murrell, S. Carter, S. C. Farantos, P. Huxley, and A. J. C. Varandas, *Molecular Potential Energy Functions* (John Wiley & Sons, Chichester, 1984).

[57] G. Herzberg, *Molecular Spectra and Molecular Structure: III. Electronic Spectra and Electronic Structure of Polyatomic Molecules* (Van Nostrand, New York, 1966).

[58] A. Kramida, Atomic Energy Levels and Spectra Bibliographic Database (version 2.0), https://physics.nist.gov/Elevbib, National Institute of Standards and Technology, Gaithersburg, MD, October 2, 2018.

[59] K. P. Huber and G. Herzberg, *Molecular Spectra and Molecular Structure: IV. Constants of Diatomic Molecules* (Van Nostrand, New York, 1979), Vol. IV.

[60] A. J. C. Varandas, "A useful triangular plot of triatomic potential energy surfaces," Chem. Phys. Lett. **138**, 455–461 (1987).

[61] A. J. C. Varandas, "Accurate combined-hyperbolic-inverse-power-representation of *ab initio* potential energy surface for the hydroperoxyl radical and dynamics study of O + OH reaction," J. Chem. Phys. **138**, 134117 (2013).

[62] P. W. Deutsch and L. A. Curtiss, "A theoretical study of triatomic carbon-silicon mixed clusters. Relative energies and binding energies," Chem. Phys. Lett. **226**, 387–391 (1994).

[63] G. A. Oyedepo, C. Peterson, and A. K. Wilson, "Accurate predictions of the energetics of silicon compounds using the multireference correlation consistent composite approach," J. Chem. Phys. **135**, 094103 (2011).

[64] M. Bogey, M. Cordonnier, C. Demuynck, and J. L. Destombes, "Millimeter- and submillimeter-wave spectroscopy of nonrigid transient molecules: Analysis of silane and acetylene plasmas," in *Structures and Conformations of Non-Rigid Molecules*, edited by J. Laane, M. Dakkouri, B. van der Veken, and H. Oberhammer (Springer Netherlands, Dordrecht, 1993), pp. 303–323.

[65] J. Tennyson, M. A. Kostin, P. Barletta, G. J. Harris, O. L. Polyansky, J. Ramanlal, and N. F. Zobov, "DVR3D: A program suite for the calculation of rotation-vibration spectra of triatomic molecules," Comput. Phys. Commun. **163**, 85–116 (2004).

[66] A. J. C. Varandas and S. P. J. Rodrigues, "A realistic double many-body expansion potential energy surface for $SO_2(\widetilde{X}^1A')$ from a multiproperty fit to accurate *ab initio* energies and vibrational levels," Spectrochim. Acta, Part A **58**, 629–647 (2002).

[67] J. Zheng, J. L. Bao, D. G. Truhlar *et al.*, "Polyrate 17-C, a computer program for the calculation of chemical reaction rates for polyatomics," https://comp.chem.umn.edu/polyrate/, University of Minnesota, Minneapolis, MN, 2017.

[68] W. L. Hase, R. J. Duchovic, X. Hu, A. Komornik, K. F. Lim, D. H. Lu, G. H. Peslherbe, K. N. Swamy, S. R. V. Linde, A. J. C. Varandas, H. Wang, and R. J. Wolf, "VENUS96: A general chemical dynamics computer program," QCPE Bull. **16**, 43 (1996).

[69] A. Zanchet, M. Agúndez, V. J. Herrero, A. Aguado, and O. Roncero, "Sulfur chemistry in the interstellar medium: The effect of vibrational excitation of H_2 in the reaction $S^+ + H_2 \rightarrow SH^+ + H$," Astrophys. J. **146**, 125 (2013).

[70] G. H. Peslherbe, H. Wang, and W. L. Hase, "Monte Carlo sampling for classical trajectory simulations," in *Advances in Chemical Physics* (Wiley-Blackwell, 1999), Chap. 6, pp. 171–201.

[71] C. M. R. Rocha and H. Linnartz, "Theoretical studies of carbon fractionation in reactions of C with C_2: Dynamics, kinetics and isotopologue equilibria," Astron. Astrophys. **647**, A142 (2021).

[72] K. J. Laidler, "The development of the Arrhenius equation," J. Chem. Educ. **61**, 494–498 (1984).

[73] J. Cernicharo, C. A. Gottlieb, M. Guelin, P. Thaddeus, and J. M. Vrtilek, "Astronomical and laboratory detection of the SiC radical," Astrophys. J., Lett. **341**, L25 (1989).

[74] D. D. S. Mackay, "SiO in dense molecular clouds reconsidered," Mon. Not. R. Astron. Soc. **278**, 62–72 (1996).

[75] E. Herbst, T. J. Millar, S. Wlodek, and D. K. Bohme, "The chemistry of silicon in dense interstellar clouds," Astron. Astrophys. **222**, 205–210 (1989).

[76] D. C. B. Whittet, W. W. Duley, and P. G. Martin, "On the abundance of silicon carbide in the interstellar medium," Mon. Not. R. Astron. Soc. **244**, 427 (1990).

[77] T. Chen, C. Y. Xiao, A. Li, and C. T. Zhou, "Where have all the interstellar silicon carbides gone?," Mon. Not. R. Astron. Soc. **509**, 5231–5236 (2021).

[78] A. J. C. Varandas and S. P. J. Rodrigues, "New double many-body expansion potential energy surface for ground-state HCN from a multiproperty fit to accurate *ab initio* energies and rovibrational calculations," J. Phys. Chem. A **110**, 485–493 (2006).